Recent advances in solid-state NMR computational spectroscopy: The case of alumino-silicate glasses

Graphical abstract.

Recent advances in solid-state NMR computational spectroscopy: the case of alumino-silicate glasses.

Alfonso Pedone

[1]Dipartimento di Scienze Chimiche e Geologiche, Università di Modena e Reggio Emilia, Via G. Campi 103, 41125 Modena, ITALIA

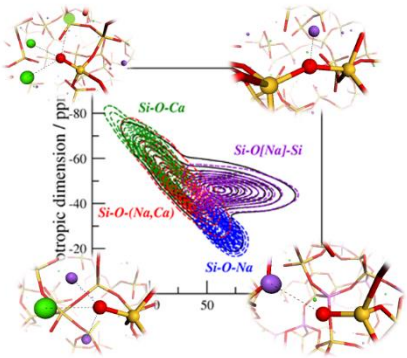

Molecular Dynamics Simulations coupled with DFT-GIPAW NMR calculations and Spin-Effective Hamiltonians provide a clear view of the local and medium range structure of multicomponent alumina silicate glasses.

Recent advances in solid-state NMR computational spectroscopy: the case of alumino-silicate glasses.

Alfonso Pedone

[1]Dipartimento di Scienze Chimiche e Geologiche, Università di Modena e Reggio Emilia, Via G. Campi 103, 41125 Modena, ITALIA

Corresponding Author

* Prof. Alfonso Pedone, [1]Dipartimento di Scienze Chimiche e Geologiche, Università di Modena e Reggio Emilia, Via G. Campi 103, 41125 Modena, ITALIA. Email: alfonso.pedone@unimore.it

Abstract.

Solid-state NMR spectroscopy and computational approaches such as Molecular Dynamics (MD) simulations and Density Functional Theory have proven to be very useful and versatile techniques for studying the structure and the dynamics of non-crystalline materials if a direct comparison between experiment and theory is established.

In this review, the basic concepts in first-principle modeling of solid-state NMR spectra of oxide glasses are presented. There are three theoretical ingredients in the computational recipe. First, classical or ab initio molecular dynamics simulations are employed to generate the structural models of the glasses of interest. Second, periodic Density Functional Theory calculations coupled with the gauge including projector augmented-wave (GIPAW) algorithm form the basis for the ab initio calculations of NMR parameters (chemical shielding and quadrupolar parameters). Finally, Spin-effective Hamiltonian are employed to simulate the solid-state NMR spectra directly comparable with the experimental counterparts.

As an example of this methodology, the investigation of the local and medium range structure of Na-Ca silicate and aluminosilicate glasses that are usually employed as simplified models for basaltic, andesitic and rhyolitic magmas will be reported. We will show how the direct comparison of the theoretical NMR spectra of MD derived structural models with the experimental counterparts allows gaining new insights into the atomistic structure of very complex oxide glasses.

Keywords

NMR-GIPAW, NMR spectra, alumino-silicate glasses, 3D structure.

Introduction

Solid-state NMR spectroscopy is one of the most important tools for investigating the atomic structure of non-crystalline materials such as oxide glasses and melts since long time.[1]

The strength of NMR spectroscopy relies on the strong correlation existing between NMR parameters and the short and medium-range structure of spin active nuclei constituting the glass.[2]

However, the orientation dependence of each nuclear spin interaction means that, for powder samples, the NMR spectrum of a given nucleus consists of a very broad powder pattern made up of an infinite number of sharp lines, one from each different molecular orientation present in the sample.

To overcome this problem and increase the spectra resolution, in the last decades much research has been focused on the development of techniques able to average the anisotropic broadening to zero, either by manipulating the spins or by manipulating the sample.

Magic Angle Spinning[3–5] (MAS) NMR has been extensively applied to cancel out the effect of dipolar and chemical shift anisotropies of spin ½ nuclei whereas dynamic angle-spinning (DAS), double rotation (DOR), or multiquantum magic-angle spinning (MQMAS) NMR techniques[6,7] have been developed to remove the second order quadrupolar effects present for nuclei with half-integer nuclear spin.

Although experiments of this kind allow a high resolution in crystalline materials, in glasses the interpretation remains difficult for several reasons. In the first place, at difference with crystalline materials in a glass the lineshape is intrinsically a powder lineshape as the glass is, from a NMR point of view, a frozen liquid. Then, the chemical and topological disorder of a glass increases with the number of constituents and the inhomogeneous broadening of the isotropic line is caused by the continuous distribution of NMR parameters arising from a continuous distribution of structural parameters.[8]

Although in the past the interpretation of the spectra was based primarily on empirical correlations derived from the study of crystalline materials with known structure recent advances in theoretical calculations of NMR parameters have proved to be very helpful in interpreting spectra of glasses.[9–12]

Earlier theoretical investigations were carried out on small molecular clusters using atomic orbital basis sets.[13,14] Nevertheless, it was soon demonstrated that the accuracy of the cluster approach in reproducing NMR observables of 3D-extended systems is limited by the size of the cluster, the termination of the dangling bonds produced on cutting the cluster from the infinite solid and the treatment of the electrostatic interactions especially in ionic solids.[14,15]

Furthermore, in the special case of amorphous materials this approach does not account for the correlations between structural factors that exist in solids and disorder in glasses.

The introduction of effective methods specially devised to calculate NMR parameters in extended systems described within periodic boundary conditions, plane wave basis sets, and density functional theory[16,17] have solved most of the aforementioned problems.

In this framework, the chemical shifts and the electric field gradients can be obtained from first principle with the gauge including projector augmented-wave (GIPAW) and the projector augmented-wave (PAW) methods, respectively,[16–18] or with methods based on localized Wannier[19] or Gaussian functions.[39]

These methods are able to deal with large systems (up to hundreds of atoms), and exhibit an outstanding accuracy, as demonstrated recently for various crystalline solids.[20–23]

In oxide glasses, the calculation of NMR parameters is not always enough for a direct comparison with experimental observables since the latter ones are usually derived from the empirical fitting of the NMR spectra, which are composed of several overlapping sub-spectra of the different structural units present in the glass. During the fitting procedure, the relative peak positions and half-band width of the different chemical sites are not precisely known and the various assumptions made do not always allow for an unambiguous interpretation.[1]

A possible way out for a direct comparison between theory and experiments and thus for a detailed interpretation of solid state spectra aided by computer experiments is to employ the computed NMR parameters to model the whole spectra by means of spin effective Hamiltonian encoded in homemade packages.[11,12]

In the last years, a collaboration between our research group with that headed by Dr. Thibault Charpentier (IRAMIS-CEA, France) has led to the development of a synergistic experimental and computational approach to investigate the structure of oxide glasses. We have developed an integrated computational method that combines Molecular Dynamics Simulations, periodic DFT calculations and Spin-effective NMR Hamiltonians which allow us to compute 1D and 2D solid state NMR spectra of all the spin-active nuclei of the periodic table.[11,12]

This approach showed to be a decisive interpretative tool for a deeper understanding of the spectral behaviour of different cations (^{27}Al,^{29}Si,^{31}P,^{43}Ca,^{23}Na) and anions (^{19}F and ^{17}O) in multicomponent oxide glasses[12,24–28] and a predictive instrument to map NMR data in a distribution of structural parameters and vice versa.[10,29]

In this review, we will describe the computational procedure employed to simulate solid-state NMR spectra and the information on the atomic structure of silicate and aluminosilicate glasses that we have gained by the application of such procedure.

Computational Procedure.

Glass Generation via Molecular Dynamics Simulations.

Unlike crystalline materials, the computational modeling of inorganic glasses is a difficult task since no currently conceivable set of experiments leads to a unique structure of an amorphous compound and thus it is not possible to obtain atomistic models (coordinates of the atoms) that reproduce the known experimental features of the system of interest. Both Monte Carlo (MC) and Molecular Dynamics techniques have been employed to generate glass structures.[30,31]

However, from a physical point of view MD simulations may be considered the most intuitive and natural way to make a computer model of an amorphous or glassy material.[32,33]

In this framework, simulated glass structures are prepared computationally in the same way as real glasses by rapidly quenching an equilibrated liquid through the glass transition and freezing the structure into a disordered glassy phase.

Of course, *ab initio* MD is ways more accurate than Classical MD, but also extremely more expensive in terms of computational time and resources. All the structural models used to simulate the NMR spectra that will be shown in this work were generated via classical MD, adopting the core-shell model for an explicit treatment of oxide ions polarizability.

A detailed description of both the cooling procedure and the force-field functional forms and parameters used are outside the scope of this review and can be found in recent literature of our group.[28,29,33,34]

Calculation of the NMR chemical shift and electric field gradients.

The first-principle calculation of NMR parameters has become more and more popular over the year, and many methods have been developed in quantum chemistry and physics community to perform such computations.

As for the chemical shift calculations, most of these methods are based on the definition of the chemical shielding tensor, as the proportional factor between the induced and the external applied magnetic field at the position of the nuclei, $\overleftrightarrow{\sigma}(\vec{R}) = dB^{ind}(\vec{R})/d\vec{B}^{ext}$.

The induced magnetic field, $\vec{B}^{ind}(\vec{r})$, is computed according to the Biot-Savart law:

$$\vec{B}^{ind}(\vec{r}) = \frac{\mu_0}{4\pi}\int d^3\vec{r}'\,\frac{\vec{r}' - \vec{r}}{|\vec{r}' - \vec{r}|^3} \times \vec{\jmath}(\vec{r}') \qquad (1)$$

Where the induced current, $\vec{\jmath}(\vec{r})$, induced by the external magnetic field, $\vec{B}^{ext}$, is obtained from the first order perturbation theory as the sum of a diamagnetic current density depending only on the unperturbed ground state wavefunction $\Phi^{(0)}$ and a paramagnetic current density, which depend on the first order correction $\Phi^{(1)}$ in the electronic ground state with respect to the unperturbed system:

$$\vec{\jmath}(\vec{r}') = \vec{\jmath}^{\,d}(\vec{r}') + \vec{\jmath}^{\,p}(\vec{r}') \qquad (2)$$

$$= \frac{e^2}{m_e}\vec{A}(\vec{r}')|\Phi^{(0)}(\vec{r}')|^2$$

$$+ \frac{e}{m_e}\left\langle \Phi^{(0)}(\vec{r}')\middle|[\hat{p}|\vec{r}'\rangle\langle\vec{r}'| + |\vec{r}'\rangle\langle\vec{r}'|\hat{p}]\middle|\Phi^{(1)}(\vec{r}')\right\rangle$$

Therefore, for calculating the shielding tensor one has to compute the current density.

However, because of the presence of the position operator on the perturbation Hamiltonian operator the latter cannot be represented under periodic boundary conditions and its expectation values are not defined for extended systems.

Until the work of Mauri et al.[35] no theory existed for the ab initio calculation of the induced current and thus most of the ab initio prediction of the NMR parameters in extended systems relied on the cluster approximation.

In their approach, Mauri et al. obtained the magnetic response to a uniform field as the long-wavelength limit of a periodically modulated field and they removed the numerical instability introduced in this limit using a sum rule.

This method was used to calculate NMR chemical shifts of light elements in an all-electron approach. Heavier nuclei required the employment of pseudopotentials and thus since the core contribution to the total chemical shift is not independent on the environment the method was thought to be not appropriate.[36] However, in later studies it was demonstrated that the total chemical shift of heavier nuclei could be well reproduced if a careful separation of individually gauge –invariant core and valence contributions is performed.[37]

In 2001, Mauri and Pickard[16] introduced the gauge including projector augmented wave (GIPAW) method. This is an extension of the projector-augmented wave (PAW) method[17] that allows calculating all-electron properties by using pseudopotential-based schemes but since it not translational invariant in the presence of a magnetic field a magnetic field dependent phase factor similar to that used in the gauge including atomic orbital (GIAO) method[38] is introduced.

In the same years, other methods to compute NMR chemical shifts and magnetic susceptibilities based on localized Wannier orbitals and Gaussian orbitals were proposed by Sebastiani and Parrinello[19] and Weber et al.,[39] respectively.

As introduced above, in addition to the NMR chemical shift, the electric field gradient tensor is another quantity of particular interest for nuclei with spin greater than one half because it defines the value of the quadrupolar coupling constants.

In principle, any first principle calculation can be employed to calculate the electric field gradient tensor $\overleftrightarrow{V}(\vec{r})$ whose definition at the position $\vec{r}$ is given by:

$$V_{\alpha\beta}(\vec{r}) = \frac{\partial E_\alpha(\vec{r})}{\partial r_\beta} - \frac{1}{3}\delta_{\alpha\beta}\sum_\gamma \frac{\partial E_\gamma(\vec{r})}{\partial r_\gamma} \quad (3)$$

where α, β and γ denote the Cartesian coordinates x, y, z and $E_\alpha(\vec{r})$ is the local electric field at the position $\vec{r}$ which can be calculated from the charge density $n(\vec{r})$:

$$E_\alpha\,(\vec{r}) = \int d^3r' \frac{n(\vec{r}')}{|\vec{r}-\vec{r}'|^3}(r_\alpha - r'_\alpha) \quad (4)$$

The EFG tensor is then equal to:

$$V_{\alpha\beta}(\vec{r}) = \int d^3r' \frac{n(\vec{r}')}{|\vec{r}-\vec{r}'|^3}\left[\delta_{\alpha\beta} - 3\frac{(r_\alpha - r'_\alpha)(r_\beta - r'_\beta)}{|\vec{r}-\vec{r}'|^2}\right] \quad (5)$$

This is a quantity frequently computed in electronic structure calculations and within the pseudopotential approach; this is efficiently done by using the PAW reconstruction scheme.[17]

Nowadays, the majority of the periodic calculations of the NMR parameters is performed by using the GIPAW and the PAW approaches which are implemented in several QM softwares[40,41] for especially devised for performing periodic DFT calculations.

Solid State NMR Spectra Simulation.

The simulation of solid-state NMR spectra is quite demanding because computational techniques must account for time-dependent modulation (sample spinning) and the summation of signals from a large number of molecular orientation (*powder averaging*). Nowadays, codes running on personal computers can provide theoretical spectra in few seconds or minutes, even taking into account all relevant interactions of the spin systems.[42–45] This paragraph provides a very concise summary of the

simulation of solid-state NMR spectra; more details can be found in the valuable series of reviews written by Mattias Edén on this topic.[46–48]

Simulation programs calculate time- or frequency-domain signal stepping through 3 main parts. The first step is called *initialization* and consists on the provision of input data on experimental conditions and spin system characteristics. The second step consists in the calculation of *spin dynamics*; that is. the evolution in time, during the NMR experiment, of the spin density operator, which describes the state of an ensemble of spin systems. Finally, in the third step (*post-processing* step) the calculated NMR signals are further processed (ex.: peak broadening) to provide the *theoretical* NMR spectra.

The core, and most time-consuming part, of the simulation is the second step. The evolution of spin systems experiencing anisotropic interactions in a rotating frame is described by the Irreducible Spherical Tensor (IST) [49–51] formalism.

Spectra simulation codes generally reconstruct the Hamiltonian representing the NMR interaction, by scalar product of IST, where each scalar product involves a *spatial* tensor, $\overleftrightarrow{\mathbf{A}}^{(\mathrm{l})}_{\mathrm{NMR}}$ and a spin tensor, which elements are spin operators represented by matrices, $\overleftrightarrow{\mathbf{T}}^{(\mathrm{l})}_{\mathrm{NMR}}$:

$$\mathbf{H}_{\mathrm{NMR}} = \mathrm{C} \sum_{\mathrm{i}=0,2} \left[\overleftrightarrow{\mathbf{A}}^{(\mathrm{l})}_{\mathrm{NMR}}\right]^{\mathrm{L}} \left[\overleftrightarrow{\mathbf{T}}^{(\mathrm{l})}_{\mathrm{NMR}}\right]^{\mathrm{L}} \qquad (6)$$

The capital letter, L, means “laboratory reference frame”, where the *z* axis coincides with the direction of the applied magnetic field, **B**.

Once the Hamiltonian for the spin system is built, the density operator carries the information about the state of an ensemble of nuclear spin systems. The Hamiltonian will cause the density operator to change throughout the NMR experiment.

The Schrödinger equation dictates how the spin density operator, and hence the nuclear spins, evolves in time and must be solved by employing an operator called the propagator. In practice, the propagator is estimated numerically and may then be used to calculate the spin density operator at any time point during the NMR experiment. The time-domain signal at a given time point is calculated as the trace of the product of an observable operator and the density operator at that given time point.

The procedure is repeated for a series of time points so that the time-domain signal, s(t), can be obtained and, subsequently, the corresponding NMR spectrum is calculated by Fourier transformation. It is worth noticing that the summarized procedure presented is referred to the generations of single molecular orientation signals in a static and rotating sample.

Glass samples for solid-state NMR spectroscopy are usually powders. Then, NMR simulation codes dedicated to glass systems must be able to simulate spectra of powders comprising a large number of microscopically small crystals, through a procedure called powder averaging. There are many fundamental equations for calculating powder averages, and reference [48] explains in details how they may be implemented on a computer, and which formalisms can be adopted to speed up the calculation. All the Solid State NMR spectra that will be shown in the next paragraphs have been generated by using an homemade code named fpNMR written by Charpentier.[11,12]

For each atomic site *i*, the NMR spectrum of interest, say $I_i(\vec{v})$, is calculated and then co-added to yield the final NMR spectrum $I(\vec{v}) = \sum_i I_i(\vec{v})$.

The general formula of a 1D-NMR spectrum for a single site is the following:

$$I(\nu) = \int d\alpha\, d\beta\, sin\beta \cdot \int dt\, e^{-2i\pi\nu t}\, e^{2i\pi\nu(\alpha,\beta)t} = \int d\alpha\, d\beta\, sin\beta \cdot \delta\{\nu - \nu(\alpha,\beta)\} \quad (7)$$

where $\nu(\alpha,\beta)$ is the NMR frequency of interest and the integration over the Euler angles (α,β), that is the powder averaging is performed by employing the Alderman's method.[52]

Finally, for 2D-NMR spectra the direct summation method where $I(v_1, v_2) = I(v_1) \times I(v_2)$ can be efficiently employed for each crystal orientation.

In the case of a broad NMR parameter distribution, as a consequence of the small number of sites that can be considered using *ab initio* NMR calculations, simulated NMR spectra, especially 2D, can exhibit strong spurious spectral features (discretization noise). Generally, as done in many other spectroscopies (IR, RAMAN,…), a convolution with a Gaussian (or other distribution) in the frequency space (ν_1,ν_2) is employed to smooth the simulated spectrum.

However, since such procedure does not accounts for possible correlation between the NMR parameters it is sometime replaced by the so-called Kernel Density Estimation (KDE) in which the NMR parameter distributions computed at the GIPAW level are smoothed by using a Gaussian Kernel and used to compute the NMR spectra.[11,12] Several works have in fact demonstrated that the KDE approach is much more powerful, especially for simulating the MQMAS spectra of Ca and Na ions as shown in **figure 1**.

The Structure of Silicate and Alumino-Silicate Glasses.

The structure of silicate and aluminosilicate glasses has been investigated in several experimental works[53–58] in order to understand the macroscopic chemico-physical properties of such systems[53,59–67] which are very important in both the technological and geological viewpoints.

The structural network of silicate glasses has been understood in terms of interconnected $(SiO_{4/2})^{4-}$ tetrahedra that are partially replaced by $(AlO_{4/2})^{5-}$ tetrahedra in aluminosilicate glasses. Non-framework cations (such as alkaline and earth-alkaline elements) can locally compensate the excess of negative charge of Al-containing networks and/or depolymerize networks by forming non-bridging oxygen atoms NBOs (i.e. oxygen atoms connected to only one network former cation).

NMR spectroscopy, being sensitive to the short- and medium-range environments of probe nuclei, is challenging for providing precious details on glass structures, like Q^n speciation of network formers, network chemical disorder, and the coordination environment of non-framework cations since each nucleus provides signals that generate spectra very rich of structural information albeit they are of difficult interpretation in some cases.

In the last years, we have employed molecular dynamics simulations, DFT-GIPAW calculations and NMR experiments to investigate the local structure around atomic species such as silicon, aluminum, oxygen, sodium and calcium of the Ca, Na silicate and aluminosilicate glasses with compositions listed in **Table 1**.

The findings relative to each specific NMR-active nucleus are briefly summarized in the separate paragraphs that follow.

^{29}Si NMR.

Silicon-29 is the only stable NMR-active Si isotope and its natural abundance is 4.67%. Its nuclear spin is I = ½, meaning that it is not a quadrupolar nucleus. Its gyromagnetic ratio, γ = -8.465 MHz·T^{-1}, allows the collection of high-quality spectra at low-medium magnetic fields (< 10 T). For these reasons, the first step in the study of the short and medium range structure of silica based glasses cannot do without the collection of ^{29}Si MAS NMR spectra.

In one of our first papers[29] we simulated the ^{29}Si MAS NMR spectra of the MD-derived NAS, CAS, CASN and CSN glass structural models and compared them with the experimental counterparts. Such comparison, which is shown in **figure 2,** allowed us to validate our models and to gain new information on the silicon environment in these glasses.

In all the structures, silicon atoms were four-fold coordinated as expected. NAS and CAS glasses exhibited the more polymerized networks whereas CASN and CSN were less polymerized. In the NAS glass, 98.3 % of silicon atoms were Q^4 species, whereas the remaining 1.7 % were in Q^3 units. In the CAS glass, a smaller amount of Q^4 (95.7%) species and a slightly higher amount of Q^3 (2.1%) and Q^2 (1.4%) species were found. In the CASN glass, 42% of silicon atoms were found in Q^4 species, 47.3% in Q^3 species and the remaining 10% in Q^2 species. The CSN glass was constituted by 8.6% of Q^4, 52.5% of Q^3, 35.2% of Q^2 and 3.1% of Q^1 species.

For CAS and CASN glasses, MD and fitted Q^n populations were in very good agreement, while CSN and NAS populations differed up to 14.8 %. Regarding the isotropic chemical shifts of such species both the theoretical and fitted δ_{iso} ranges from about -100 ppm to -70 ppm and differed of 1-2 ppm.

After having investigated the first coordination sphere of silicon we focused on the Si/Al intermixing in its second coordination sphere; that is, the so-called framework chemical disorder. In particular, we observed that the δ_{iso} and chemical shift anisotropy (expressed in absolute values) both increased

with the number of aluminum cations in the silicon second coordination sphere. The extent of increase of δ_{iso} varied from + 2.9 to + 6.6 ppm per aluminum, and from +1.3 to + 8.8 ppm in the case of the anisotropic chemical shift parameter.

These results were used to de-convolute the NMR spectra of the NAS glass in terms of Si(Q^4)[*m*Al] species, where $m = 0 \div 4$ is the number of Al bonded to the central Q^4 Si species through a BO. The relative Si(Q^4)[*m*Al] populations and isotropic chemical shifts obtained from the fitting of ^{29}Si MAS spectra are reported in **Table 2**. The experimental isotropic chemical shifts compared quite well with those computed at the DFT-GIPAW level on the MD-derived structures whereas the comparison of the Si(Q^4)[*m*Al] species found in real samples revealed that the MD structural models underestimated the Al/Si intermixing.

As for the Na/Ca intermixing in the second coordination sphere of silicon, we observed that Ca cations are mainly allocated around Q^1 and Q^2 species, whereas Na is more localized around Q^3 and Q^4 species.

Since the knowledge of accurate relationships between NMR parameters and structural properties are extremely useful for extracting structural data from the experimental spectra[11,68–70] we also investigated the correlation between ^{29}Si δ_{iso} and Si-O-T intertetrahedral angles. **Figure 3** shows that ^{29}Si δ_{iso} differently correlates with the average Si-O-T angle depending on the Q^n speciation. It is worth noticing that, as previously observed experimentally[71] and theoretically,[25] the worst correlations were observed for the Ca-containing glasses.

^{27}Al NMR.

Aluminum-27 is the only stable isotope of Al element and is an NMR-active quadrupolar nucleus with spin I = 5/2. Because of the very high natural abundance (> 99.9 %) and the relatively low gyromagnetic ratio, $\gamma = 11.103$ MHz·T^{-1}, it is quite easy to collect high-quality MAS and 3Q-MAS spectra without isotopic enrichment of samples at medium intensity applied magnetic fields.

In a recent works,[29,72] we simulated both types of spectra for all the aluminum containing CAS, NAS, and CASN glasses and compared them with the experimental counterparts in order to validate the aluminum environment in our MD-structural models. **Figure 4** clearly shows that the computed ^{27}Al MAS NMR spectra of such glasses are peaked at about 60 ppm in perfect agreement with the experimental ones.

In our structural models, all the Al atoms were four-fold coordinated and present as Q^4 species, except for CAS models in which 5.32% of five-fold Al and 2.66 % of Al in Q^3 species were found. Our calculations showed that if 5-coordinated Al atoms are present in the glass, they could be easily distinguished from 4-coordinated Al atoms in a MAS spectrum because their δ_{iso} and C_Q values lie at around 20 ppm and 11.7 MHz, respectively. Instead, Al(Q^3) species are not well distinguishable from Al(Q^4) units by a ^{27}Al MAS spectra since its signal overlaps with the one due to Q^4 species.

The theoretical line shape of the NAS glass was broader than the experimental counterpart because our MD models overestimated the number of Al engaged in small rings and thus they have narrow inter-tetrahedra Al-O-T angles (where T= Al, Si)[73,74] and larger quadrupolar constants. The theoretical spectra of the CAS glass presents a shoulder at lower chemical shifts associated to aluminum atoms directly bonded to TBOs, which distort AlO_4 units.

Figure 4b shows that our models well reproduce the NMR parameter distribution $\pi(C_Q,\delta_{iso})$ for CAS and CASN glasses but not for the NAS glass because the models overestimate the amount of Al-TBO bonds and of Al-O-Al bridges.

We also found that ^{27}Al δ_{iso} and C_Q tends to decrease with the number of Si atoms in Al second coordination sphere.

Finally, we studied the correlation between ^{27}Al δ_{iso} and Al-O-T angles, finding that in analogy to the case of silicon the correlation worsens with the presence of Ca ions in the composition.

^{17}O NMR

^{17}O MAS and MQMAS experiments are probably the most powerful instruments for the characterization of a glass overall structure since O is the *linking* atom of the network, and coordinates both framework and non-framework cations.

In a recent paper, we simulated ^{17}O MAS and 3QMAS spectra of the glasses reported in **Table 1** in order to validate the MD structural models and to investigate the local structure around oxygen atoms. **Figure 5** reports the comparison between the theoretical and experimental spectra of the silicate glasses, CS, NS and CSN**.**

The figure clearly shows that the signals of the Si–O–Na and Si–O–Si sites are overlapped in MAS spectra and cannot be easily revolved while the signals of the Si–O–Ca and Si–O–Si ones can be distinguished since they lie in different zones. Instead, the detection of Si-O-Ca, Si-O-Si and Si-O-Na sites in NS and CS glasses is quite straightforward since their peaks are well resolved in the theoretical 3QMAS spectra.

Our calculations also showed that the Si–O–(Na,Ca) signals completely overlap with the Si–O–Ca and Si–O–Na ones and thus it is extremely difficult to extract the relative populations of the different oxygen sites for the CSN glass even from ^{17}O 3QMAS spectrum.

However, since our structural models provided spectra in good agreement with the experimental ones they reasonably reproduced also the site populations. In these models, we observed an extensive mixing of Ca and Na around NBO in soda-lime silicate glasses whereas BOs were mainly surrounded by sodium ions rather than by calcium. The most common environments found around NBO and BO in the CSN glass are shown in **Figure 6**.

As for oxygen environment in aluminosilicate glasses, we also showed that the overall shape of the spectra of the MD-derived structural models (not reported in this review) well reproduced the experimental ones available in the literature.

Although, CAS and NAS glasses have a tectosilicate composition our MD simulations showed an incomplete polymerization of both glasses and the presence of NBOs and TBOs in the system in

agreement with previous high resolution 3QMAS NMR experiments.[54] Interestingly, all the NBOs present in the three glasses were associated with Si atoms rather than Al ones.

As for TBOs, the CAS glass contained a higher amount of them (4.9%) with respect to NAS glass (1.7%) and thus we deduced that higher field strength cations promote the formation of NBO and TBO.

Among the TBOs found in our models, we showed that the NMR parameters of the OAl_2Si and $OAlSi_2$ sites fall in the same range covered by those of the Si–O–Si and Si–O–Al sites and are not detectable by ^{17}O MAS and 3QMAS NMR experiments. Conversely, OAl_3 sites (where 2 Al are involved in a 2-membered ring) can be distinguished if present in real samples.[54]

Finally, we have not been able to find simple and accurate relationships between NMR parameters and local information such as Si–O distances and Si–O–T angles. Therefore, it seems that for an unambiguous interpretation of very complex multicomponent systems the generation of structural models of glasses by means of MD simulations and the subsequent DFT-GIPAW calculations of the ^{17}O NMR parameters remains mandatory.

^{23}Na NMR.

^{23}Na NMR spectroscopy and MD-GIPAW calculations were used to investigate the Na–O coordination number and its partitioning between BO and NBO. In fact, the BO/NBO ratio around Na reflects the role played by the cation among network modifier (preferentially surrounded by NBOs) and the charge compensator (preferentially surrounded by BOs).

The reliability of Na-environment in the MD-derived CASN and CSN structural models was demonstrated by comparing the DFT-GIPAW distributions of C_Q and δ_{iso} NMR parameters $\Pi(C_Q, \delta_{iso})$ with those extracted by fitting the ^{23}Na 3QMAS spectra. Such comparison is shown in **Figure 7**. Our models well reproduced the shape of $\Pi(C_Q, \delta_{iso})$ distributions even though the theoretical distributions were shifted of +2 MHz in the C_Q axis with respect to the experimental ones.

We ascribed the systematic overestimation of the ^{23}Na C_Q computed values to the coupling between EFG of the Na^+ with its vibrational modes that was not taken into account in our calculations. However, we showed that by multiplying the theoretical C_Q values for a scaling factor of 0.47 we were able to well reproduce the $p(C_Q, \eta_Q, \delta_{iso})$ distributions of the CSN and CASN glasses as shown in **Figure 7**.

We also investigated the relationships between the ^{23}Na NMR parameters, the coordination number and the average Na–O distances as shown in **Figure 8**.

We could not find any unambiguous correlation between the ^{23}Na δ_{iso} and CN but we observed that a linear correlation between ^{23}Na δ_{iso} and the average Na–O distances was observed when different CNs were taken into account.

The theoretical NMR values found for the different NaO_n sites were used to perform a constrained fitting of experimental ^{23}Na 3QMAS spectra from which the average coordination number of Na ions was estimated.

Albeit the coordination number of Na ions was similar for both silicate and aluminosilicate glasses the determination of the BO/NBO ratio confirmed that sodium plays a charge compensator role in Ca, Na aluminosilicate glasses and a network modifier role in Ca, Na silicate glasses.

^{43}Ca NMR.

^{43}Ca is a quadrupolar nucleus (spin = 7/2) with a very low natural abundance (0.135%) and a small gyromagnetic ratio (γ) and thus it has a very low NMR sensitivity with respect to more abundant and high-γ nuclei, such as ^{23}Na or ^{27}Al. ^{43}Ca NMR experiments requires high magnetic fields, long acquisition times and isotope enrichment. Therefore, the investigation of Ca environment is difficult and expensive.[75] Consequently, a very limited number of NMR reports for the ^{43}Ca nucleus can be found in literature. [75,76]

The first investigation of Ca environment in silicate and aluminosilicate glass was performed by Shimoda et al.[76] by using 3Q, 5Q and 7QMAS experiments and identified three distinct peaks that

were associated to Ca atoms coordinated by 6, 7 and 8 oxygen atoms. The average coordination number increased from 7.1 in $CaSiO_3$ glass to 7.8 in $CaAl_2Si_2O_8$ glass. However, in a subsequent work we showed that MD derived structural models with Ca coordination environment ranging from 5 to 8 CN well reproduced both the MAS and MQMAS spectra of $CaSiO_3$ glass.[12]

As for aluminosilicate glasses, we investigated the sensitivity of ^{43}Ca NMR parameters toward the structural role played by Ca by using both MAS and 3QMAS experiments collected at a magnetic field of 11.7 T and MD-GIPAW calculations.[28]

In our structural models, Ca was coordinated by 5.7, 5.8 and 5.3 oxygens in CAS, CASN and CSN glasses, respectively. We observed that Ca acts as charge compensator in CAS glass and as network modifier in CASN glass.

Analogously to sodium, ^{43}Ca δ_{iso} better correlates with the average Ca-O distances when the coordination number is taken into account but it does not correlate with the coordination number.

In contrast to the case of ^{23}Na, we have not been able to obtain an estimation of the population of the different Ca sites and to estimate the average Ca-O bond distances because of the low signal to noise ratio of the acquired ^{43}Ca 3QMAS spectra.

However, by exploiting the empirical correlation shown in **figure 9** between ^{43}Ca δ_{iso} and the average Ca-O distance proposed by Angeli et al. and elaborated on crystalline samples[77] we estimated average Ca-O distances of 2.54 Å, 2.46 Å and 2.40 Å for CAS, CASN and CSN, respectively.

Concluding Remarks

In this review, we have highlighted the potentiality of the MD-GIPAW computational protocol when combined with solid-state NMR experiments, and have provided an overall descriptions of silicate and aluminosilicate glass structural features provided by computational NMR spectroscopy and MD-derived models.

The interpretative and predictive abilities of the protocol developed in the last years encouraged its employment to other families of multicomponent glasses for a detailed characterization of their short- and medium-range environment.

However, the method itself needs improvements on both computational efficiency of DFT calculations and theoretical formalism.

In fact, lower computational costs would allow getting wider sets of theoretical spectroscopic and structural data, which could be obtained by generating larger models. These sets would be an ideal starting point for the evaluation of those multivariate correlations that are necessary to perform reliable *structural inversions* of NMR experimental data sets to achieve structural information directly from NMR spectra.

Moreover, we saw that ^{23}Na C_Q values are systematically overestimated because thermal effects are not taken into account by the protocol. Thus, there is a clear need for developing and implementing computational strategies capable of taking into account even those motions that NMR is sensitive to, like micro/millisecond time motions. A further improvement of DFT-GIPAW needs to account for relativistic effects, making the design of improved XC functional a key task.

Finally, I hope to have shown that the combination of MD and GIPAW calculations holds a promising prospect for providing both structural and dynamical information in amorphous solids.

Acknowledgements.

The author thanks all the collaborators with which he has worked in the past in the simulation of solid state NMR spectra of oxide glasses. In particular, Dr. Thibault Charpentier, Dr. Elisa Gambuzzi and Prof. Maria Cristina Menziani.

References.

1. H. Eckert, *Prog. Nucl. Magn. Reson. Spectrosc.*, **1992**, 24, 159–293.

2. M. Edén, *Annu. Rep. Sect. C Phys. Chem.*, **2012**, 108, 177–221.
3. E. Dupree and R. F. Pettifer, *Nature*, **1984**, 308, 523–525.
4. H. Eckert, J. H. Kennedy, A. Pradel and M. Ribes, *J. Non-Cryst. Solids*, **1989**, 113, 287–293.
5. H. Maekawa, T. Maekawa, K. Kawamura and T. Yokokawa, *J. Non-Cryst. Solids*, **1991**, 127, 53–64.
6. L. Frydman and J. S. Harwood, *J. Am. Chem. Soc.*, **1995**, 117, 5367–5368.
7. A. Medek, J. S. Harwood and L. Frydman, *J. Am. Chem. Soc.*, **1995**, 117, 12779–12787.
8. P. Zhang, P. J. Grandinetti and J. F. Stebbins, *J. Phys. Chem. B*, **1997**, 101, 4004–4008.
9. T. Charpentier, *Solid State Nucl. Magn. Reson.*, **2011**, 40, 1–20.
10. T. Charpentier, M. C. Menziani and A. Pedone, *Rsc Adv.*, **2013**, 3, 10550–10578.
11. T. Charpentier, P. Kroll and F. Mauri, *J. Phys. Chem. C*, **2009**, 113, 7917–7929.
12. A. Pedone, T. Charpentier and M. C. Menziani, *Phys. Chem. Chem. Phys.*, **2010**, 12, 6054–6066.
13. J. A. Tossell and J. Horbach, *J. Phys. Chem. B*, **2005**, 109, 1794–1797.
14. A. Pedone, M. Pavone, M. C. Menziani and V. Barone, *J. Chem. Theory Comput.*, **2008**, 4, 2130–2140.
15. A. Pedone, M. Biczysko and V. Barone, *Chemphyschem*, **2010**, 11, 1812–1832.
16. C. J. Pickard and F. Mauri, *Phys. Rev. B*, **2001**, 63, 245101.
17. M. Profeta, F. Mauri and C. J. Pickard, *J. Am. Chem. Soc.*, **2003**, 125, 541–548.
18. J. R. Yates, C. J. Pickard and F. Mauri, *Phys. Rev. B*, **2007**, 76, 024401.
19. D. Sebastiani and M. Parrinello, *J. Phys. Chem. A*, **2001**, 105, 1951–1958.
20. M. Profeta, M. Benoit, F. Mauri and C. J. Pickard, *J. Am. Chem. Soc.*, **2004**, 126, 12628–12635.
21. G. Ferlat, T. Charpentier, A. P. Seitsonen, A. Takada, M. Lazzeri, L. Cormier, G. Calas and F. Mauri, *Phys. Rev. Lett.*, **2008**, 101, 065504.
22. C. Ferrara, C. Tealdi, A. Pedone, M. C. Menziani, A. J. Rossini, G. Pintacuda and P. Mustarelli, *J. Phys. Chem. C*, **2013**, 117, 23451–23458.
23. D. Presti, A. Pedone and M. C. Menziani, *Inorg. Chem.*, **2014**, 53, 7926–7935.

24. A. Pedone, T. Charpentier and M. C. Menziani, *J. Mater. Chem.*, **2012**, 22, 12599–12608.
25. A. Pedone, T. Charpentier, G. Malavasi and M. C. Menziani, *Chem. Mater.*, **2010**, 22, 5644–5652.
26. A. Pedone, E. Gambuzzi and M. C. Menziani, *J. Phys. Chem. C*, **2012**, 116, 14599–14609.
27. E. Gambuzzi, T. Charpentier, M. C. Menziani and A. Pedone, *Chem. Phys. Lett.*, **2014**, 612, 56–61.
28. E. Gambuzzi, A. Pedone, M. C. Menziani, F. Angeli, P. Florian and T. Charpentier, *Solid State Nucl. Magn. Reson.*
29. E. Gambuzzi, A. Pedone, M. C. Menziani, F. Angeli, D. Caurant and T. Charpentier, *Geochim. Cosmochim. Acta*, **2014**, 125, 170–185.
30. C. R. A. Catlow, B. Smit and R. A. van Santen, *Computer Modelling of Microporous Materials*, Academic Press, **2004**.
31. D. A. Keen and R. L. McGreevy, *Nature*, **1990**, 344, 423–425.
32. J. Du, in *Molecular Dynamics Simulations of Disordered Materials*, eds. C. Massobrio, J. Du, M. Bernasconi and P. S. Salmon, Springer International Publishing, **2015**, pp. 157–180.
33. A. Pedone, *J. Phys. Chem. C*, **2009**, 113, 20773–20784.
34. E. Gambuzzi and A. Pedone, *Phys. Chem. Chem. Phys.*, **2014**, 16, 21645–21656.
35. F. Mauri and S. G. Louie, *Phys. Rev. Lett.*, **1996**, 76, 4246–4249.
36. P. Diehl, E. Fluck and R. Kosfeld, *NMR Basic Principles and Progress / NMR Grundlagen und Fortschritte*, Springer Science & Business Media, **2012**.
37. T. Gregor, F. Mauri and R. Car, *J. Chem. Phys.*, **1999**, 111, 1815–1822.
38. R. Ditchfield, *Mol. Phys.*, **1974**, 27, 789–807.
39. V. Weber, M. Iannuzzi, S. Giani, J. Hutter, R. Declerck and M. Waroquier, *J. Chem. Phys.*, **2009**, 131, 014106.
40. S. J. Clark, M. D. Segall, C. J. Pickard, P. J. Hasnip, M. I. J. Probert, K. Refson and M. C. Payne, *Z. Für Krist.*, **2005**, 220, 567–570.

41. P. Giannozzi, S. Baroni, N. Bonini, M. Calandra, R. Car, C. Cavazzoni, D. Ceresoli, G. L. Chiarotti, M. Cococcioni, I. Dabo, A. D. Corso, S. de Gironcoli, S. Fabris, G. Fratesi, R. Gebauer, U. Gerstmann, C. Gougoussis, A. Kokalj, M. Lazzeri, L. Martin-Samos, N. Marzari, F. Mauri, R. Mazzarello, S. Paolini, A. Pasquarello, L. Paulatto, C. Sbraccia, S. Scandolo, G. Sclauzero, A. P. Seitsonen, A. Smogunov, P. Umari and R. M. Wentzcovitch, *J. Phys. Condens. Matter*, **2009**, 21, 395502.
42. M. Bak, J. T. Rasmussen and N. C. Nielsen, *J. Magn. Reson.*, **2000**, 147, 296–330.
43. T. Charpentier, C. Fermon and J. Virlet, *J. Magn. Reson.*, **1998**, 132, 181–190.
44. M. Hohwy, H. Bildsøe, H. J. Jakobsen and N. C. Nielsen, *J. Magn. Reson.*, **1999**, 136, 6–14.
45. M. Veshtort and R. G. Griffin, *J. Magn. Reson. San Diego Calif 1997*, **2006**, 178, 248–282.
46. M. Edén, *Concepts Magn. Reson.*, **2003**, 17A, 117–154.
47. M. Edén, *Concepts Magn. Reson.*, **2003**, 18A, 1–23.
48. M. Edén, *Concepts Magn. Reson.*, **2003**, 18A, 24–55.
49. D. W. Alderman, M. H. Sherwood and D. M. Grant, *J. Magn. Reson. A*, **1993**, 101, 188–197.
50. M. Mehring and V. A. Weberruss, *Object-oriented magnetic resonance classes and objects, calculations and computations*, Academic Press, San Diego, Calif., **2001**.
51. V. J. McBrierty, *Nuclear magnetic resonance in solid polymers*, Cambridge University Press, Cambridge ; New York, Digitally printed 1st pbk. version., **2006**.
52. D. W. Alderman, M. S. Solum and D. M. Grant, *J. Chem. Phys.*, **1986**, 84, 3717–3725.
53. P. Duxson, J. L. Provis, G. C. Lukey, F. Separovic and J. S. J. van Deventer, *Langmuir*, **2005**, 21, 3028–3036.
54. J. F. Stebbins and Z. Xu, *Nature*, **1997**, 390, 60–62.
55. D. R. Neuville, L. Cormier, V. Montouillout and D. Massiot, *J. Non-Cryst. Solids*, **2007**, 353, 180–184.
56. R. G. Kuryaeva, *Glass Phys. Chem.*, **2006**, 32, 505–510.
57. G. S. Henderson, D. R. Neuville and L. Cormier, *Chem. Geol.*, **2009**, 259, 54–62.

58. B. O. Mysen and P. Richet, *Silicate glasses and melts properties and structure*, Elsevier, Amsterdam; Boston, **2005**.
59. L. Cormier and D. R. Neuville, *Chem. Geol.*, **2004**, 213, 103–113.
60. P. McMillian, *Am Min.*, **1984**, 69, 622–644.
61. D. R. Neuville and B. O. Mysen, *Geochim. Cosmochim. Acta*, **1996**, 60, 1727–1737.
62. M. J. Toplis, Dingwell, Donald B., K.-W. Hess and T. Lenci, *Am Min.*, **1997**, 82, 979–990.
63. V. K. Leko and O. V. Mazurin, *Glass Phys Chem*, **2003**, 29, 16–27.
64. X. Xue, M. Kanzaki, D. R. Neuville and T. Kawamoto, *Geochim. Cosmochim. Acta*, **2004**, 68, 5011.
65. J. L. Provis, P. Duxson, G. C. Lukey and J. S. J. van Deventer, *Chem. Mater.*, **2005**, 17, 2976–2986.
66. D. Neuville, *Chem. Geol.*, **2006**, 229, 28–41.
67. P. Richet, A. Nidaira, D. R. Neuville and T. Atake, *Geochim. Cosmochim. Acta*, **2009**, 73, 3894–3904.
68. T. M. Clark, P. J. Grandinetti, P. Florian and J. F. Stebbins, *Phys. Rev. B*, **2004**, 70, 064202.
69. F. Angeli, O. Villain, S. Schuller, S. Ispas and T. Charpentier, *Geochim. Cosmochim. Acta*, **2011**, 75, 2453–2469.
70. A. Soleilhavoup, J.-M. Delaye, F. Angeli, D. Caurant and T. Charpentier, *Magn. Reson. Chem.*, **2010**, 48, S159–S170.
71. P. Florian, F. Fayon and D. Massiot, *J. Phys. Chem. C*, **2009**, 113, 2562–2572.
72. A. Pedone, E. Gambuzzi, G. Malavasi and M. C. Menziani, *Theor. Chem. Acc.*, **2012**, 131, 1–11.
73. E. Lippmaa, A. Samoson and M. Magi, *J. Am. Chem. Soc.*, **1986**, 108, 1730–1735.
74. F. Angeli, J.-M. Delaye, T. Charpentier, J.-C. Petit, D. Ghaleb and P. Faucon, *Chem. Phys. Lett.*, **2000**, 320, 681–687.
75. D. Laurencin and M. E. Smith, *Prog. Nucl. Magn. Reson. Spectrosc.*, **2013**, 68, 1–40.

76. K. Shimoda, Y. Tobu, Y. Shimoikeda, T. Nemoto and K. Saito, *J. Magn. Reson.*, **2007**, 186, 156–159.

77. R. Dupree, A. P. Howes and S. C. Kohn, *Chem. Phys. Lett.*, **1997**, 276, 399–404.

Figures.

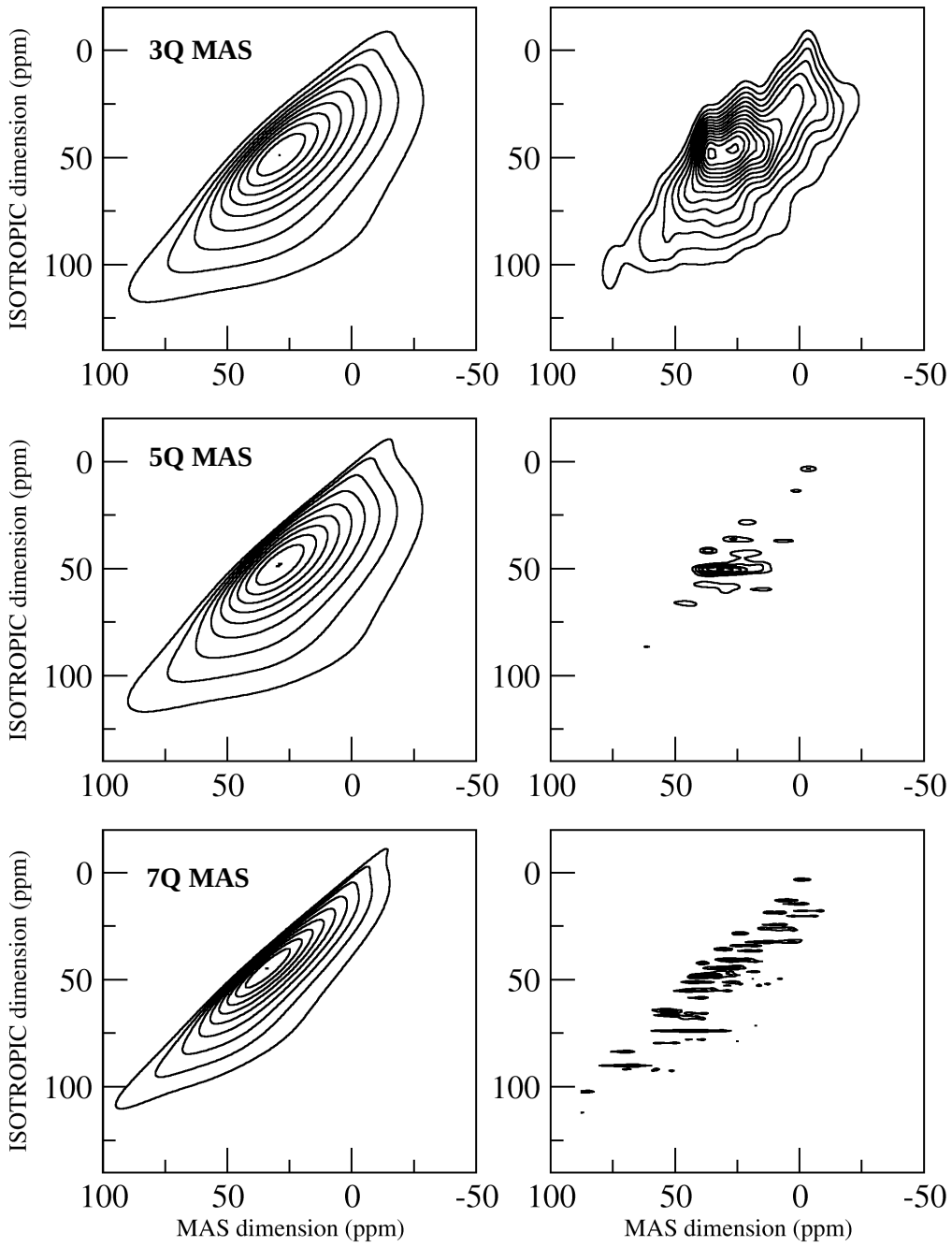

Figure 1. KDE (left) vs Direct (right) ^{43}Ca MQMAS spectra for mq=3,5 (16.4T) and mq=7 (21.8T) of the CaSiO3 glass model. Reproduced from Ref.[12] with permission from the PCCP Owner Societies.

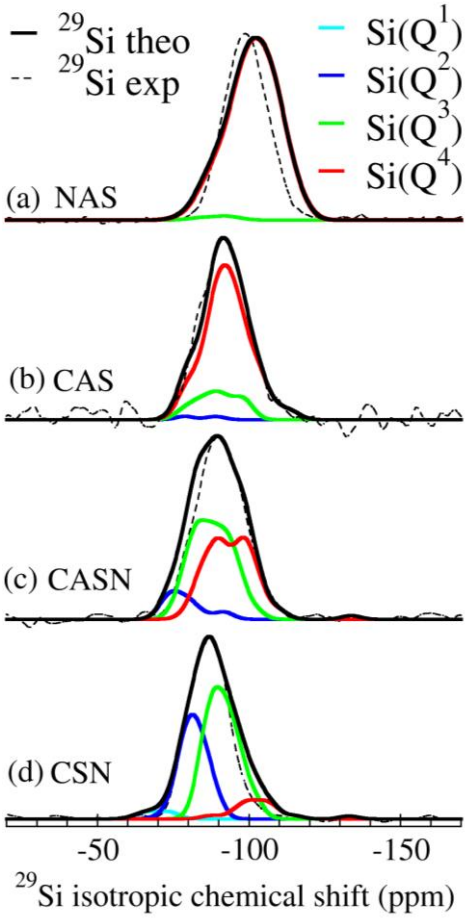

Figure 2. Comparison between experimental (black dashed lines) and theoretical (black solid lines) ^{29}Si MAS NMR spectra (normalized to the same maximum height) of NAS (a), CAS (b) and CASN (c) and CSN (d) glasses. Simulated individual contribution of Q^n species to the total theoretical spectra are reported in colored solid lines. Figure is reproduced from ref.[29] with permission from Elsevier.

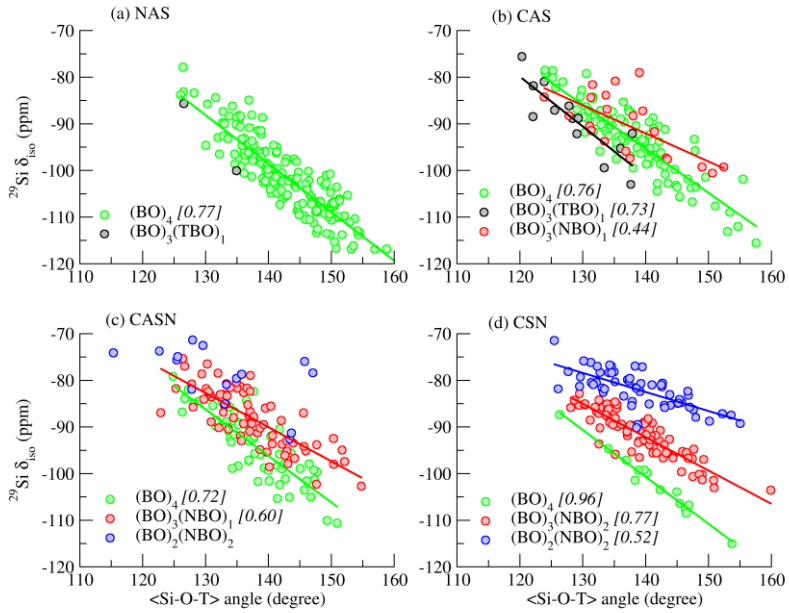

Figure 3. Plot of ^{29}Si δ_{iso} vs <Si-O-T> reported for different connectivity environments of Si in NAS, CAS, CASN and CSN. $Si(BO)_4$ are green dots, $Si(BO)_3(NBO)_1$ are red dots, $Si(BO)_2(NBO)_2$ are blue dots and $Si(BO)_3(TBO)_1$ are black circles. Linear regression fitting lines are also reported with coherent colors and coefficients of determination of linear regression, R^2, are listed in brackets. Reproduced from ref. [29] with permission from Elsevier.

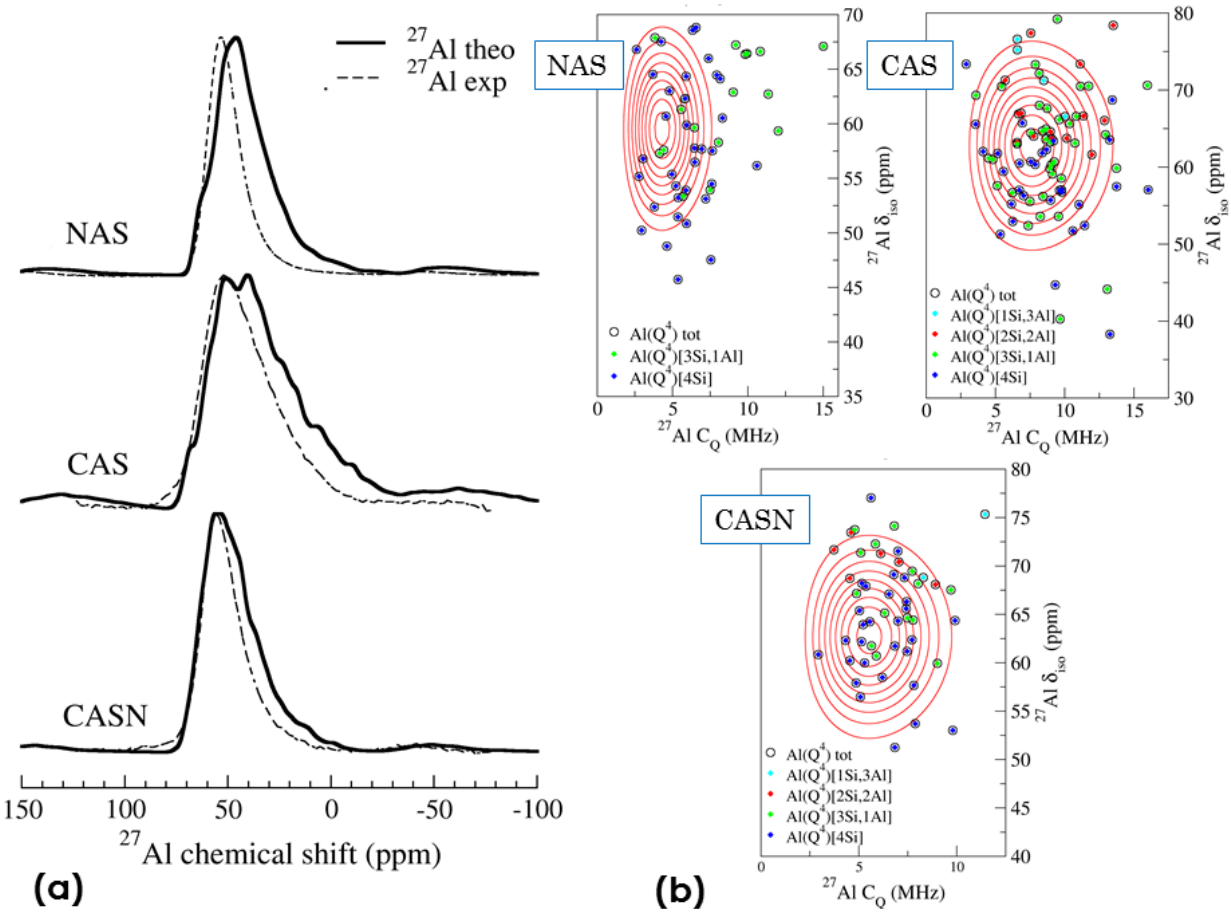

Figure 4. (a) Comparison between normalized experimental spectra (collected at a magnetic field of 11.7 T, dashed lines) and computed (black solid lines) ^{27}Al MAS NMR spectra of NAS, CAS and CASN aluminosilicate glasses. (b) $\Pi(C_Q,\delta_{iso})$ distribution of NAS, CAS and CASN glasses: fitted from experiment (dashed lines) and theoretical counterparts derived from DFT calculations on MD derived models (symbols). Different symbols represent different Al(Q^4) sites, and refer to the speciation of Al(Q^4) in Al(Q^4)[jSi,4 − jAl] species. Figure (a) is reproduced from ref[29] with permission from Elsevier.

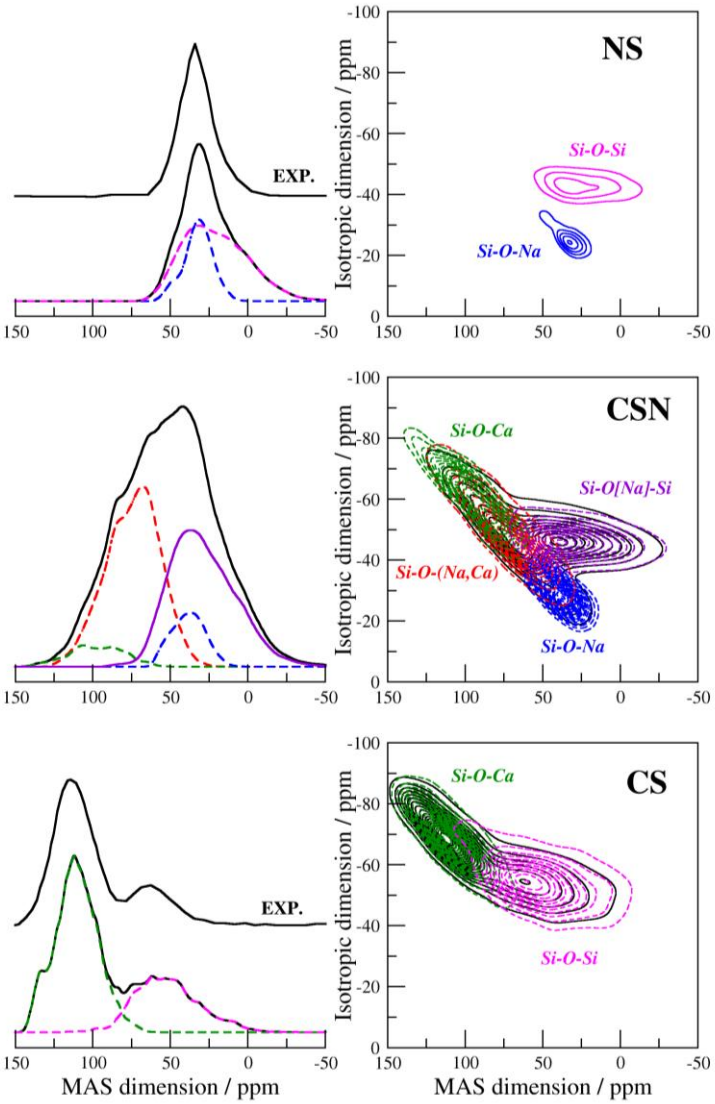

Figure 5. (left) Computed ^{17}O MAS and (right) 3QMAS spectra of the NS, CSN and CS glasses. The experimental ^{17}O MAS spectra are also reported for the NS[3] and CS[70] glasses. Reproduced from ref.[26] with permission from American Chemical Society.

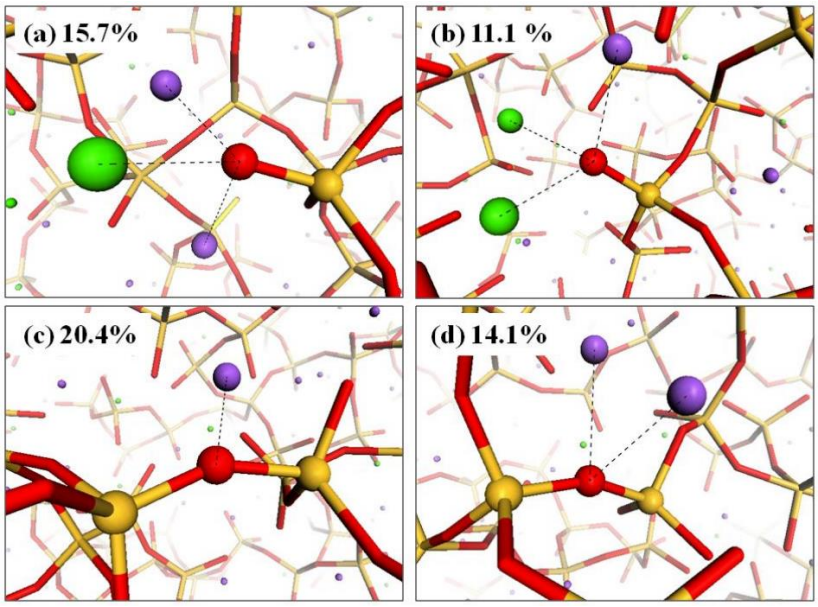

Figure 6. The most common oxygen environments in the CSN glass: (a) Si-NBO(1Ca,2Na), (b) Si-NBO(2Ca,1Na), (c) Si-BO(1Na)-Si and (d) Si-BO(2Na)-Si sites. Oxygens, sodium and calcium atoms are represented as red, violet and green spheres. Silicon atoms are represented as yellow sticks.

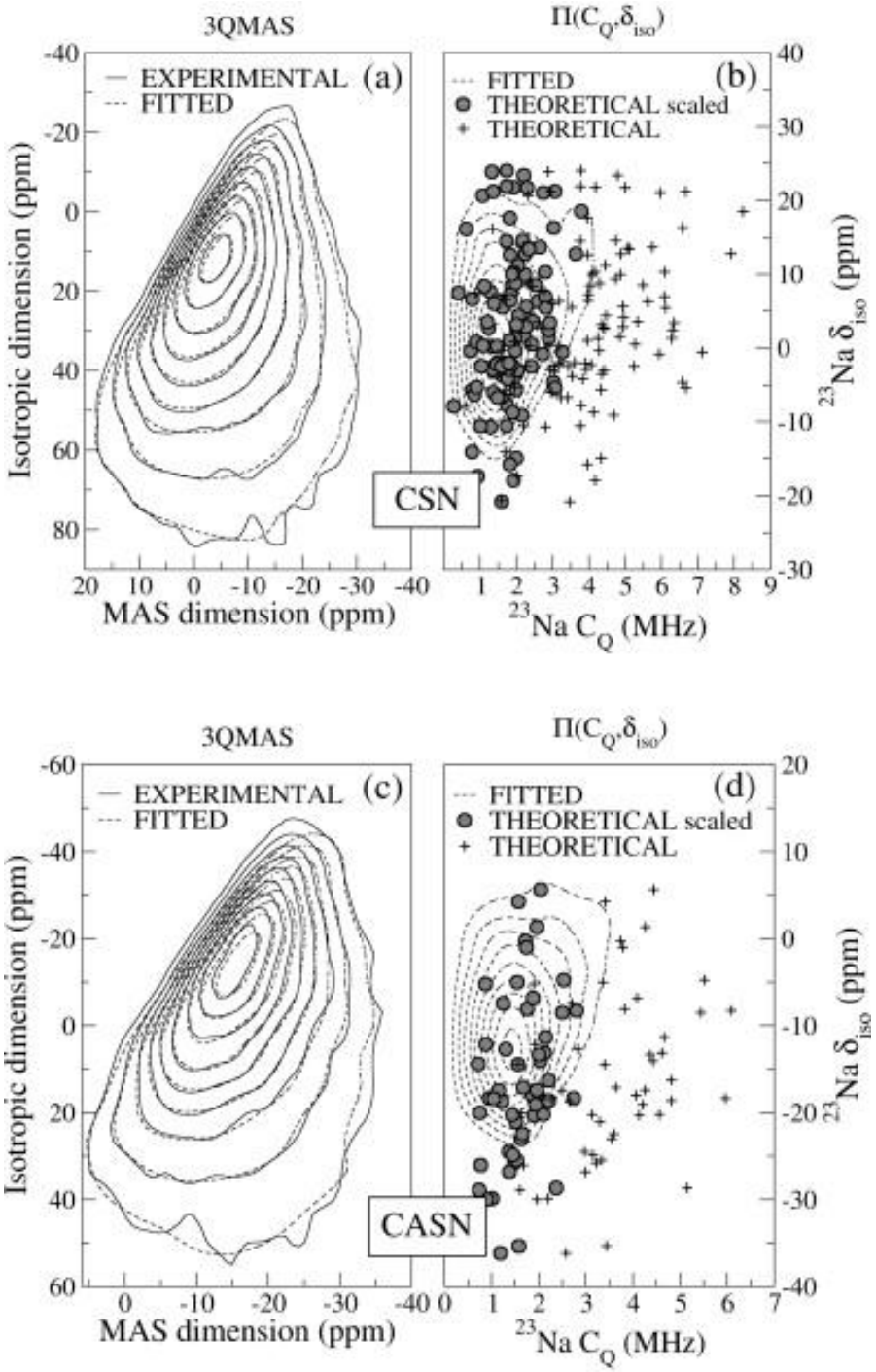

Figure 7. ^{23}Na 3QMAS experimental spectra of CSN (a) and CASN (c) glasses (solid lines) and simulated spectra via fitting procedure (dashed lines); $\Pi(C_Q, \delta_{iso})$ distributions of CSN (b) and CASN (d) glasses: fitted from experiment (dashed lines) and theoretical counterparts derived from DFT calculations on MD derived models (dots). Figure is reproduced from ref.[27] with permission from Elsevier.

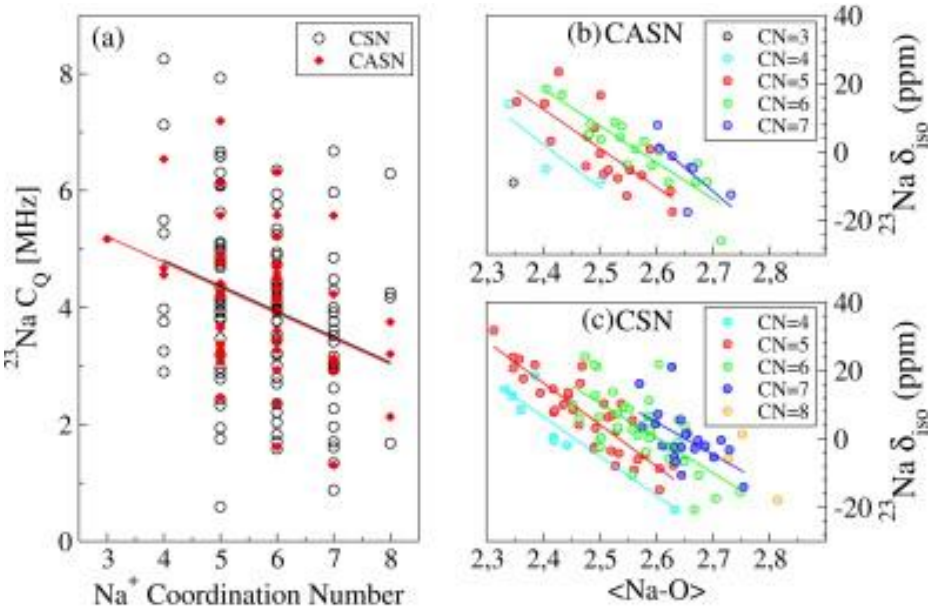

Figure 8. Variation of ^{23}Na NMR parameters as a function of some short-range structural features: (a) ^{23}Na C_Q vs Na^+ CN in CSN and CASN, trend lines are reported for visual guide; ^{23}Na δ_{iso} vs average Na-O distance, <Na-O>, for CASN (b) and CSN (c), where Na atoms are differentiated with respect to their CN. Figure is reproduced from ref.[27] with permission from Elsevier.

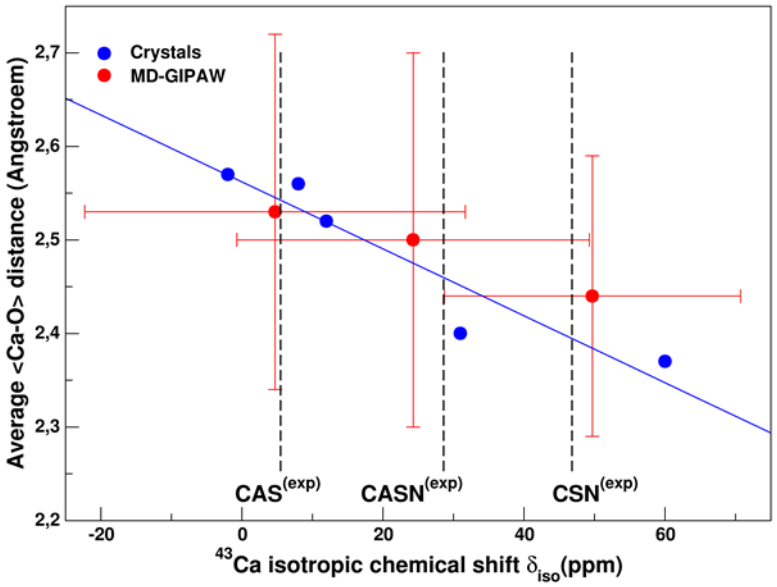

Figure 9. Correlation between <Ca-O> and ^{43}Ca δ_{iso} elaborated on crystalline samples (blue). <Ca-O> from MD-derived models (red) and ^{43}Ca δ_{iso} obtained in this work from MQMAS spectra (dashed lines). For MD data, error bars represents width (standard deviation value) of the distribution. Figure is reproduced from ref.[28]with permission from Elsevier.

Tables.

Table 1. Composition (mol%) of the glasses.

Glasses		SiO_2	Al_2O_3	Na_2O	CaO
silicate	CS	50%	---	---	50%
	NS	75%	---	25%	---
	CSN	60%	---	20%	20%
aluminosilicate	NAS	78%	11%	11%	---
	CAS	60%	20%	---	20%
	CASN	60%	10%	10%	20%

Table 2. Quantification of chemical disorder of NAS network: fitting experimental spectra with $Si(Q^n)[mAl]$ (n = 3,4; m = 0÷3) species constraints.

Species	Pop %, $_{EXP}$[(a)]	$\delta_{iso,\ EXP}$[(a)] (ppm)
Si	100.0	103.0(5.9)
$Si(Q^4)[0Al]$	68.8	-105.6(5.9)
$Si(Q^4)[1Al]$	21.3	-102.8(5.9)
$Si(Q^4)[2Al]$	0.0	-95.4(5.9)
$Si(Q^4)[3Al]$	9.9	-85.8(5.9)
$Si(Q^3)[0Al]$	0.0	-89.7(5.0)

[(a)] Error associated to fitting procedure: 0.27 %.

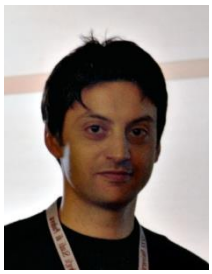

Alfonso Pedone received his degree and Ph. D in chemistry at the University of Modena and Reggio Emilia, where currently is Associate Professor in Physical Chemistry. He conducts research in the field of computer simulations based on classical, quantum mechanical and multiscale methods applied to the study of inorganic materials, organic molecular crystals and nanomaterials. He has co-authored more than 80 papers published in international journals and 5 book chapters.